Research Article | Vol. 8, No. 12 | 1 Dec 2017 | BIOMEDICAL OPTICS EXPRESS 5412
Biomedical Optics EXPRESS

Two-photon laser scanning microscopy with electrowetting-based prism scanning

Omkar D. Supekar,[1,*] Baris N. Ozbay,[2] Mo Zohrabi,[3] Philip D. Nystrom,[1] Gregory L. Futia,[2] Diego Restrepo,[4] Emily A. Gibson,[2] Juliet T. Gopinath,[3,5] and Victor M. Bright[1]

[1]*Department of Mechanical Engineering, University of Colorado, Boulder, CO, 80309, USA*
[2]*Department of Bioengineering, University of Colorado Anschutz Medical Campus, Aurora, Colorado, 80045, USA*
[3]*Department of Electrical, Computer, and Energy Engineering, University of Colorado, Boulder, CO, 80309, USA*
[4]*Department of Cell and Developmental Biology, University of Colorado Anschutz Medical Campus, Aurora, Colorado, 80045, USA*
[5]*Department of Physics, University of Colorado, Boulder, CO 80309-0390, USA*
[*]*omkar.supekar@colorado.edu*

Abstract: Laser scanners are an integral part of high resolution biomedical imaging systems such as confocal or 2-photon excitation (2PE) microscopes. In this work, we demonstrate the utility of electrowetting on dielectric (EWOD) prisms as a lateral laser-scanning element integrated in a conventional 2PE microscope. To the best of our knowledge, this is the first such demonstration for EWOD prisms. EWOD devices provide a transmissive, low power consuming, and compact alternative to conventional adaptive optics, and hence this technology has tremendous potential. We demonstrate 2PE microscope imaging of cultured mouse hippocampal neurons with a FOV of 130 × 130 μm^2 using EWOD prism scanning. In addition, we show simulations of the optical system with the EWOD prism, to evaluate the effect of propagating a Gaussian beam through the EWOD prism on the imaging quality. Based on the simulation results a beam size of 0.91 mm full width half max was chosen to conduct the imaging experiments, resulting in a numerical aperture of 0.17 of the imaging system.

OCIS codes: (010.1080) Active or adaptive optics; (230.5480) Prisms; (230.2090) Electro-optical devices; (170.0110) Imaging systems; (170.2520) Fluorescence microscopy; (180.5810) Scanning microscopy.

References and links

1. S. R. Schultz, C. S. Copeland, A. J. Foust, P. Quicke, and R. Schuck, "Advances in two photon scanning and scanless microscopy technologies for functional neural circuit imaging," Proc. IEEE Inst. Electr. Electron. Eng. **105**(1), 139–157 (2017).
2. W. C. Warger and C. A. DiMarzio, "Dual-wedge scanning confocal reflectance microscope," Opt. Lett. **32**(15), 2140–2142 (2007).
3. R. Salomé, Y. Kremer, S. Dieudonné, J. F. Léger, O. Krichevsky, C. Wyart, D. Chatenay, and L. Bourdieu, "Ultrafast random-access scanning in two-photon microscopy using acousto-optic deflectors," J. Neurosci. Methods **154**(1-2), 161–174 (2006).
4. W. Denk, J. H. Strickler, and W. W. Webb, "Two-photon laser scanning fluorescence microscopy," Science **248**(4951), 73–76 (1990).
5. F. Helmchen and W. Denk, "Deep tissue two-photon microscopy," Nat. Methods **2**(12), 932–940 (2005).
6. K. Svoboda and R. Yasuda, "Principles of two-photon excitation microscopy and its applications to neuroscience," Neuron **50**(6), 823–839 (2006).
7. T.-W. Chen, T. J. Wardill, Y. Sun, S. R. Pulver, S. L. Renninger, A. Baohan, E. R. Schreiter, R. A. Kerr, M. B. Orger, V. Jayaraman, L. L. Looger, K. Svoboda, and D. S. Kim, "Ultrasensitive fluorescent proteins for imaging neuronal activity," Nature **499**(7458), 295–300 (2013).
8. M. E. Bocarsly, W. C. Jiang, C. Wang, J. T. Dudman, N. Ji, and Y. Aponte, "Minimally invasive microendoscopy system for in vivo functional imaging of deep nuclei in the mouse brain," Biomed. Opt. Express **6**(11), 4546–4556 (2015).
9. W. Yang and R. Yuste, "In vivo imaging of neural activity," Nat. Methods **14**(4), 349–359 (2017).

#308690 https://doi.org/10.1364/BOE.8.005412
Journal © 2017 Received 6 Oct 2017; revised 31 Oct 2017; accepted 2 Nov 2017; published 7 Nov 2017

Biomedical Optics EXPRESS

10. J. Sawinski, D. J. Wallace, D. S. Greenberg, S. Grossmann, W. Denk, and J. N. D. Kerr, "Visually evoked activity in cortical cells imaged in freely moving animals," Proc. Natl. Acad. Sci. U.S.A. **106**(46), 19557–19562 (2009).
11. W. Zong, R. Wu, M. Li, Y. Hu, Y. Li, J. Li, H. Rong, H. Wu, Y. Xu, Y. Lu, H. Jia, M. Fan, Z. Zhou, Y. Zhang, A. Wang, L. Chen, and H. Cheng, "Fast high-resolution miniature two-photon microscopy for brain imaging in freely behaving mice," Nat. Methods **14**(7), 713–719 (2017).
12. F. Helmchen, W. Denk, and J. N. D. Kerr, "Miniaturization of two-photon microscopy for imaging in freely moving animals," Cold Spring Harb. Protoc. **2013**(10), 904–913 (2013).
13. F. Helmchen, "Miniaturization of fluorescence microscopes using fibre optics," Exp. Physiol. **87**(6), 737–745 (2002).
14. F. Helmchen, M. S. Fee, D. W. Tank, and W. Denk, "A miniature head-mounted two-photon microscope. high-resolution brain imaging in freely moving animals," Neuron **31**(6), 903–912 (2001).
15. M. T. Myaing, D. J. MacDonald, and X. Li, "Fiber-optic scanning two-photon fluorescence endoscope," Opt. Lett. **31**(8), 1076–1078 (2006).
16. D. Bird and M. Gu, "Two-photon fluorescence endoscopy with a micro-optic scanning head," Opt. Lett. **28**(17), 1552–1554 (2003).
17. W. Göbel, J. N. D. Kerr, A. Nimmerjahn, and F. Helmchen, "Miniaturized two-photon microscope based on a flexible coherent fiber bundle and a gradient-index lens objective," Opt. Lett. **29**(21), 2521–2523 (2004).
18. F. Mugele and J.-C. Baret, "Electrowetting: from basics to applications," J. Phys. Condens. Matter **17**, R705–R774 (2005).
19. B. Berge and J. Peseux, "Variable focal lens controlled by an external voltage: An application of electrowetting," Eur. Phys. J. E **3**, 159–163 (2000).
20. S. Kuiper and B. H. W. Hendriks, "Variable-focus liquid lens for miniature cameras," Appl. Phys. Lett. **85**, 1128–1130 (2004).
21. A. Shahini, J. Xia, Z. Zhou, Y. Zhao, and M. M. C. Cheng, "Versatile miniature tunable liquid lenses using transparent graphene electrodes," Langmuir **32**(6), 1658–1665 (2016).
22. A. Shahini, H. Jin, Z. Zhou, Y. Zhao, P. Y. Chen, J. Hua, and M. M. Cheng, "Toward individually tunable compound eyes with transparent graphene electrode," Bioinspir. Biomim. **12**(4), 046002 (2017).
23. D. Kopp, L. Lehmann, and H. Zappe, "Optofluidic laser scanner based on a rotating liquid prism," Appl. Opt. **55**(9), 2136–2142 (2016).
24. N. R. Smith, D. C. Abeysinghe, J. W. Haus, and J. Heikenfeld, "Agile wide-angle beam steering with electrowetting microprisms," Opt. Express **14**(14), 6557–6563 (2006).
25. A. Takei, E. Iwase, K. Hoshino, K. Matsumoto, and I. Shimoyama, "Angle-tunable liquid wedge prism driven by electrowetting," J. Microelectromech. Syst. **16**, 1537–1542 (2007).
26. S. Terrab, A. M. Watson, C. Roath, J. T. Gopinath, and V. M. Bright, "Adaptive electrowetting lens-prism element," Opt. Express **23**(20), 25838–25845 (2015).
27. S. Murali, K. P. Thompson, and J. P. Rolland, "Three-dimensional adaptive microscopy using embedded liquid lens," Opt. Lett. **34**(2), 145–147 (2009).
28. B. N. Ozbay, J. T. Losacco, R. Cormack, R. Weir, V. M. Bright, J. T. Gopinath, D. Restrepo, and E. A. Gibson, "Miniaturized fiber-coupled confocal fluorescence microscope with an electrowetting variable focus lens using no moving parts," Opt. Lett. **40**(11), 2553–2556 (2015).
29. O. D. Supekar, M. Zohrabi, J. T. Gopinath, and V. M. Bright, "Enhanced response time of electrowetting lenses with shaped input voltage functions," Langmuir **33**(19), 4863–4869 (2017).
30. S. Preibisch, S. Saalfeld, J. Schindelin, and P. Tomancak, "Software for bead-based registration of selective plane illumination microscopy data," Nat. Methods **7**(6), 418–419 (2010).
31. M. Zohrabi, R. H. Cormack, and J. T. Gopinath, "Wide-angle nonmechanical beam steering using liquid lenses," Opt. Express **24**(21), 23798–23809 (2016).

1. Introduction

An important component of high resolution microscopes is a scanner for the light source, in order to build up an image. Standard microscopes utilize mirrors controlled by moving magnet galvanometers (galvo mirrors) [1]. Raster scanning through galvo mirrors is achieved by driving two mirrors in orthogonal rotation axes, with one of the mirrors assigned to the fast axis while the other scans the slow axis. The fast axis scanner can also be used in resonance mode with kHz range resonance frequencies to reduce the imaging scan time. Additional transmissive laser scanning techniques such as Risley prisms [2], and acousto-optic beam deflectors [3] have also been demonstrated for high resolution microscopy. However, with growing interest in miniature microscopes for *in vivo* neuronal imaging, there is room for developing alternative technology that can be integrated into the microscope objective to provide lateral and axial laser scanning. Transmissive adaptive optics based on electrowetting on dielectric (EWOD) technology offer an attractive solution, with simplicity and low cost.

Biomedical Optics EXPRESS

The electrowetting principle enables control of the curvature of a liquid interface with an applied voltage, enabling tunable liquid lenses, prisms and customizable surfaces.

In particular, this work is focused on applying our innovative scanning technique to two-photon excitation microscopy (2PE). Since its invention [4], 2PE has become a powerful tool for high-resolution, deep tissue imaging [5,6]. With recent developments in ultrasensitive fluorescence indicators [7], 2PE microscopy has gained significant traction for high resolution *in vivo* neuronal stimulation and readout [8,9] in freely behaving mice [10–12]. Laser scanning for miniature 2PE microscopes using single mode fibers has been shown with piezoelectric fiber tip scanning [13–15], and rotating microprism scanners [16]. Unfortunately, this technology cannot be truly miniaturized and can require significant electrical power. Scanning the distal end of a fiber bundle can solve these problems [17], but the image resolution suffers. In contrast, our solution of an electrowetting prism millimeters in size, with mW of electrical power consumption, is an exciting choice.

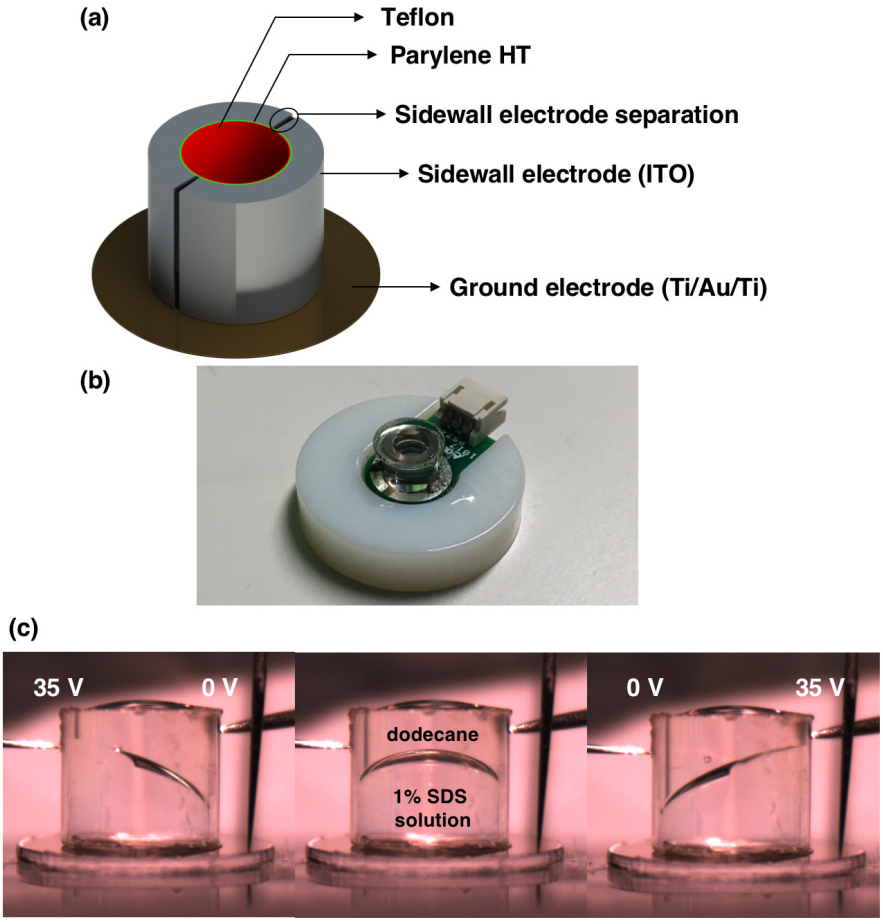

Fig. 1. Device fabrication, packaging and operation. (a) Schematic of the device with components labeled. An optical window with patterned Ti/Au/Ti layer serves as the ground electrode. The device is constructed in a cylindrical glass tube with ITO sidewall electrodes, Parylene HT as the dielectric and Teflon as the hydrophobic layer. (b) An image of the device bonded to the custom 3D printed mount, with liquids filled and capped with an optical window. (c) Demonstration of the device functioning as a tunable prism, (center) device functioning as a diverging lens with no applied voltage, (left) 35 V applied to the left sidewall, and (right) 35 V applied to the right sidewall. Ti/Au/Ti = Titanium/Gold/Titanium; ITO = Indium Tin Oxide.

Biomedical Optics EXPRESS

In an electrowetting device, an applied electric field changes the contact angle of a polar liquid on a substrate. The electric field is generated by applying a voltage between the polar liquid and an underlying electrode across a dielectric surface [18]. The contact angle variation on the surface with applied voltage is given by the Lippmann-Young equation.

$$\cos\theta = \cos\theta_0 + \frac{\epsilon_0 \epsilon_{eff}}{2 d_{eff} \gamma} V^2 \quad (1)$$

where θ_0 is the initial contact angle on the surface, V is the applied voltage, and γ is the surface tension between the polar liquid-ambient fluid interface. To maximize tuning, the initial contact angle can be increased by applying a hydrophobic layer on the dielectric. The effective relative permittivity and thickness of the dielectric and hydrophobic layer stack are given by ε_{eff} and d_{eff}, respectively. Changing the contact angle uniformly enables a tunable spherical liquid surface that can be used as an adaptive lens, while selectively changing the contact angle on parts of the dielectric surface enables additional control of liquid profiles, such as for tunable liquid prisms.

EWOD devices are appealing due to low power consumption, large tuning range without mechanical moving parts, and compactness. Optical elements based on this principle are used as variable focus lenses for miniature cameras [19,20], and as flexible variable focus lenses [21] and arrays [22] for compound lens systems. Recent studies on EWOD devices as adaptive prisms for non-mechanical beam steering [23–26] show great promise for their use as scanning elements in microscopy and remote sensing applications. EWOD technology has been implemented in high resolution microscopy, in microscope objectives [27] and into fiber coupled microscopes (FCM) for depth scanning [28]. The integration of EWOD prisms as an active lateral scanning element in this work for tissue imaging is the next step in developing this technology for 2PE microscopy and a step towards a 2PE-FCM system with integrated EWOD based adaptive lateral and axial scanning system.

In our work, we have demonstrated EWOD prism devices with repeatable and consistent scanning of ± 2.35° at 650 nm. To demonstrate the feasibility of EWOD prisms as laser scanning elements for 2PE microscopy, the device is integrated into a conventional 2PE microscope as a slow axis scanner. The device upon integration with the microscope, is capable of providing ± 2° of scanning at a wavelength of 950 nm with scanning speeds as fast as 21°/sec. To the best of our knowledge, this is the first demonstration of integration of an EWOD prism device as a lateral scanning element in a 2PE microscope.

2. Experimental methods

2.1 Device fabrication

The EWOD prism devices are fabricated in cylindrical glass tubes with 4 mm inner diameter and 5 mm height. A novel 3D printing-assisted shadow masking technique is used to obtain two separated sidewall electrodes required for 1D beam steering through the prism. The shadow mask is 3D printed using an Objet30 Pro (Stratasys Ltd.) polyjet printer, and produces electrodes with a 0.5 mm spacing. Using a DC sputter deposition process, 400 nm of Indium Tin Oxide (ITO) is deposited on the sidewalls of the glass tube, to serve as sidewall electrodes. After the sputter deposition process, the 3D printed part is removed and the glass tube with separated electrodes is cleaned. Before the dielectric layers are deposited, the exterior of the glass tubes is masked with Kapton tape. This is followed by vapor phase deposition of 1.2 μm of Parylene HT (Specialty Coating Systems) on the inside of the cylinder. Next, the glass tube is dip-coated in a 1:5 (by weight) solution of Teflon (Dupont, AF-1601 6%) in FC-40 (Flourinert) and cured at 170 °C for 20 min, to provide a hydrophobic coating inside the cylinder. Separately, Titanium/Gold/Titanium (Ti/Au/Ti, 20 nm/500 nm/20 nm) is evaporated and patterned on an optical window of diameter 10 mm and thickness 550 μm. This serves as the ground electrode for the electrowetting device. The optical window is

Biomedical Optics EXPRESS

custom cut from fused silica wafers using a laser cutter (Epilog Legend 36EXT). The annular electrode pattern consists of a 3.75 mm clear aperture in the optical window. Next, a 50 μm layer of SU-8 3050 is spun and patterned on top of the ground electrode. The SU-8 serves as a bonding layer to the cylindrical glass tube as well as an insulating layer between the ground and sidewall electrodes. The glass tube and optical windows are bonded together using a UV sensitive epoxy UVS-91 (Norland Products). Next, a patterned printed circuit board is aligned and placed on the device, facilitating easy access to electrode connections to the device via JST connectors. For ease of optical alignment, the device is then bonded to a custom 1" 3D printed mount. Next, the liquids (1 wt% Sodium dodecyl sulfate solution and dodecane) are filled into the device using a micropipette followed by a clear optical window of diameter 8 mm and thickness 550 μm placed on top of the device. This packaging strategy provides a seal for about 6 hours, and the ability to refill the liquids upon the introduction of air bubbles. A schematic of the EWOD device components, with images of the device and operation is shown in Fig. 1. The fabrication process flow enables devices with over 10,000 actuation cycles observed during the course of imaging experiments.

2.2 Optical setup

A tunable mode-locked Ti:Sapphire laser (Spectra-Physics, Mai Tai HP DeepSee) with a pulse width of 90 fs (full width half max, FWHM) at 950 nm was used as the excitation source. The collimated output beam from the laser has a diameter (FWHM) of 1.43 mm and can be decreased to 0.91 mm diameter (FWHM) using a reverse Galilean telescope consisting of a doublet lens with focal length −40 mm (Thorlabs ACN254-040-B) and a plano-convex lens with focal length, 75 mm (Thorlabs LA1608-B). The telescope is followed by a two-electrode EWOD prism, which provides steering, but also behaves as a diverging lens, with its focal length changing upon actuation. To remove this artifact, a commercially available variable focus EWOD lens, Artic 316 (Varioptic) is placed before the prism. The EWOD prism is actuated with a custom multichannel linear amplifier controlled using a voltage output module (National Instruments, NI-9264), and the EWOD lens (Arctic 316) is driven with a VPS-3 (Varioptic) power supply. The EWOD prism is used for beam scanning on one scan axis, while the other axis is scanned using a galvo mirror. The resulting scanned beam from the EWOD prism is relayed to a galvo mirror using a 1:1 telescope built using two 125 mm focal length achromatic doublets (Thorlabs AC254-125-B).

The angle scanning beam is translated into position scanning using a 50 mm Olympus scan lens. This position scanning beam is then imaged onto the sample plane with a microscope (Olympus IX71) composed of a 180 mm tube lens and a 20X objective (Olympus 20x/0.75NA UPlanSApo). A diagram of this system is shown in Fig. 2.

After the tube lens the excitation beam passes through a long pass dichroic with cutoff at 670 nm (Chroma T670LPXR) on its way to the objective. The 2PE generated at the sample plane is then collected by the objective and reflected off the long pass dichroic and through a 180 mm tube lens to the input plane of detection optics. These optics collimate the emission beam with a 50 mm focal length achromatic doublet (Thorlabs AC254-50-A). The excitation light not fully removed by the first dichroic is further rejected with a 785 nm razor edge filter (Semrock). A dichroic filter (Semrock FF562-Di02) with cutoff at 562 nm splits this beam enabling the capability to perform simultaneous dual detection of green and red fluorescent proteins, for example GCamp6 and tdTomato, eGFP and mCherry etc. The green emission that is reflected off the dichroic is passed through a 530/43 nm bandpass filter (Semrock) and is focused with a 25 mm focal length lens (Thorlabs LB1761-A) onto a photomultiplier tube (PMT), while the red emission that is transmitted through second dichroic is focused using a 25 mm focal length lens (Thorlabs LB1761-A) onto the second PMT. Both PMTs are Hamamatsu H7422PA-40 which have a 5 mm detector diameter. The output electrical pulses from the PMTs pass through high-bandwidth amplifiers (Becker & Hickl GmBH ACA-4-35db) and are converted to logic-level pulses by a timing discriminator (6915, Phillips

Biomedical Optics EXPRESS

Scientific). The pulses are counted by a data-acquisition (DAQ) card (National Instruments PCIe-6259) at a rate of 20 MHz. The excitation and detection systems are integrated into a custom software in LabVIEW (National Instruments) to control the galvo-mirror and the EWOD prism, and sample and bin the PMT counts by pixels to convert them into an image.

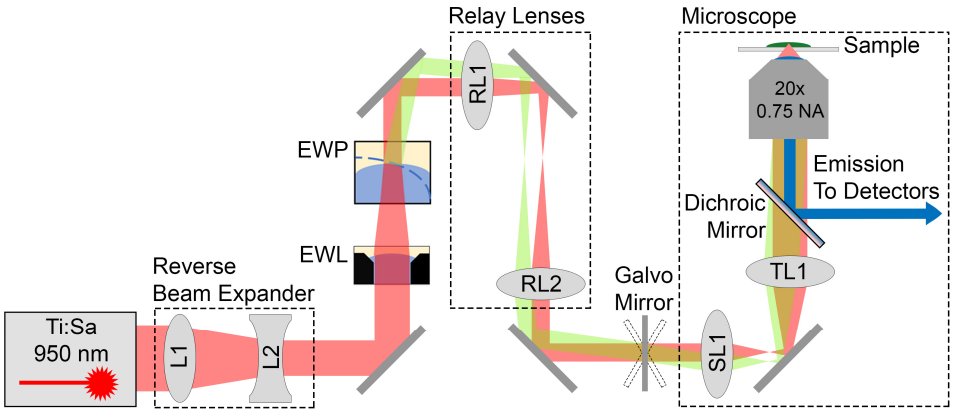

Fig. 2. Schematic of the imaging setup. A mode-locked Ti:Sapphire laser (Spectra-Physics, Mai Tai HP DeepSee) at an output wavelength of 950 nm is used as the excitation source. The reverse beam expander is used to reduce the beam size to 0.91 mm FWHM. Lens 1 (L1) focal length = 75 mm. Lens 2 (L2) focal length = –40 mm. A commercially available EWOD lens (EWL) (Arctic 316) is placed right before the EWOD prism to compensate for the focal length change during EWOD prism (EWP) actuation. The green beam indicates the scanned beam from the EWOD prism upon actuation. Relay lenses are used to relay the scan angle from the EWOD prism onto the galvo mirror plane. Relay lens 1 (RL1) and 2 (RL2) focal length = 125 mm. The microscope Olympus IX71 body contains a scan lens (SL), focal length = 50 mm, and tube lens (TL), focal length = 180 mm, system required for lateral scanning through the objective (Olympus 20X/0.75 UPlanSApo). FWHM = Full width half max.

3. Simulation setup

Zemax optical design software was used to evaluate the effects of propagating a Gaussian beam through the EWOD prism in isolation from the rest of the optics in the imaging system. The Gaussian profile of the 950 nm pulsed beam with and without the Galilean telescope was first measured using a CCD camera (Mightex), and then fit to a Gaussian function. The beam size (FWHM) without the Galilean telescope was 1.43 mm. When reduced in size by the telescope, the beam size (FWHM) was measured to be 0.91 mm. To minimize the influence of stray apertures and other optics, the galvo scanner and relay lenses were removed and the EWOD prism was placed at the back focal length of the scan lens. Further, the scan lens, tube lens, and objective lens were replaced by paraxial lenses with the same focal length. A schematic for the simulation setup is shown in Fig. 3. The EWOD tunable lens was modeled using a Zemax model provided by the manufacturer, Varioptic. The EWOD prism actuation surfaces were simulated in COMSOL Multiphysics using the Laminar two-phase flow module. The EWOD prism liquid-liquid interface surfaces were calculated as a function of applied voltage from 0V to 35V in 5V increments. The resulting surface meshes were fit to the first 11 Zernike polynomials, which were imported into Zemax as Zernike Fringe Sag surfaces at the EWOD prism liquid-liquid interface. The propagating Gaussian beam at the two beam sizes used in the experiments, as well as several other beam sizes, were modeled using the Physical Optics Propagation analysis tool and evaluated at the focus of the objective lens.

Biomedical Optics EXPRESS

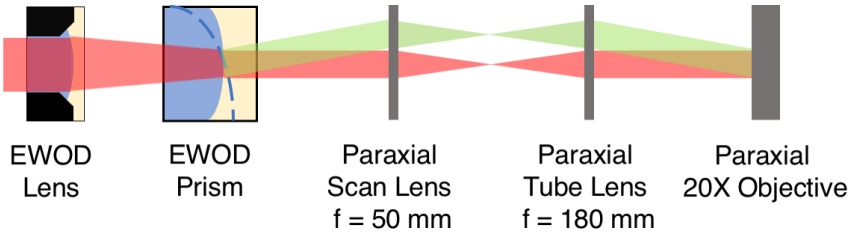

Fig. 3. Schematic of the simulation setup. EWOD lens, followed by the EWOD prism. The green beam indicates the scanned beam from the EWOD prism upon actuation. In the simulation setup, the galvo scanner and relay lenses are removed. The scan lens, tube lens, and the objective are replaced by paraxial lenses with the same focal length. EWOD = Electrowetting on dielectric.

4. Results and discussion

4.1 EWOD prism scan angle calibration

The steady-state scan angle of the EWOD prism was first characterized as a function of applied voltage on each sidewall electrode. The scan angle variation with applied voltage is dependent on the refractive index ratio between dodecane and 1% SDS solution. While the refractive index of the liquids is dependent on wavelength, it was determined that the ratio of the refractive index of the liquids increases by less than 0.5% between 650 nm and 950 nm wavelengths. This difference in the refractive index ratio would correspond to a less than 0.5% decrease in the scan angle. Hence, the scan angle characterization was performed using a 650 nm cw laser diode (Thorlabs L650P007). A beam with a 1 mm diameter (FWHM) was passed through the device and imaged onto a CCD camera (Dataray, WinCAMD-UCD12). Since the EWOD prism acts as a diverging lens, a commercially available tunable converging lens (Optotune EL-10-30) was placed before the EWOD prism to focus the beam spot on the CCD camera. The device was actuated by actuating each electrode from 0 to 35 V DC while keeping the other electrode at 0 V. The scan angle was calculated by monitoring the beam motion on the CCD camera with applied voltage. The scan angle experiments were performed with 5 independent runs to demonstrate device repeatability. The data in Fig. 4(a) shows ± 2.35° of scanning from the device. Additionally, the position of the beam spot on the camera with voltage provides information on the straightness of the scan from the EWOD prism. Figure 4(b) shows the average beam spot location for all applied voltages for the 5 runs and as expected the scanning follows a straight line with an R-squared fit of 0.998. The error bars in both Fig. 4(a) and (b) correspond to a ± 1 standard deviation of the measured results, indicating consistent scanning from the device.

Biomedical Optics EXPRESS

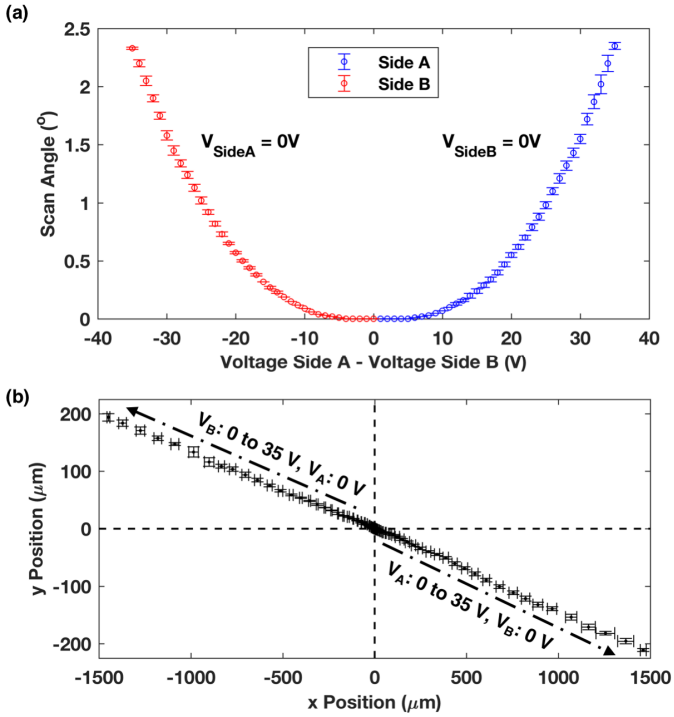

Fig. 4. (a) EWOD prism scanning as a function of applied voltage. It is evident that the scanning is very consistent on both the directions and repeatable. (b) Beam spot position on camera for all actuating voltages, the scan follows a straight line fit with an R-squared value of 0.998; The error bars indicate the standard deviation of the experimental results. EWOD = Electrowetting on dielectric.

The scan angle variation provides information on the steady-state scan angle vs. applied voltage. Based on this scan angle characterization, a time dependent voltage function of the form,

$$V(t) = 19.56\left(\theta(t)\right)^{0.4949} + 5 \tag{2}$$

was fit to the experimental data in an effort to minimize the time dependent nonlinearity of the scan angle variation.

4.2 Simulation of Gaussian beam propagation through 2PE system

The EWOD prism was modeled in a simplified version of the experimental 2PE imaging system to estimate the effects on the laser beam due to the varying surface curvature, and determine an optimal beam diameter for the imaging system. Additionally, the model was also used to simulate the change in focal length of the EWOD prism upon actuation using a Gaussian beam with a FWHM of 0.91 mm, replicating the experimental beam after the Galilean telescope. The Gaussian beam was evaluated at the front focal length of the objective and the focal length of the modeled EWOD lens was optimized to maximize the peak irradiance, indicating the tightest focus. Figure 5(a) shows the modeled EWOD lens and EWOD prism system at various scan angles. Figure 5(b) shows the EWOD lens focal length needed to compensate for the shifting focal length of the EWOD prism as a function of voltage. Figure 5(c) shows the same plot, but as a function of actuation angle, indicating that the focal length shift of the EWOD prism is approximately linearly dependent on the actuation angle. Overall, these results estimate that the effective focal length of the EWOD prism ranges from −53.2 mm at 0 V to −62.8 mm at 35 V.

Biomedical Optics EXPRESS

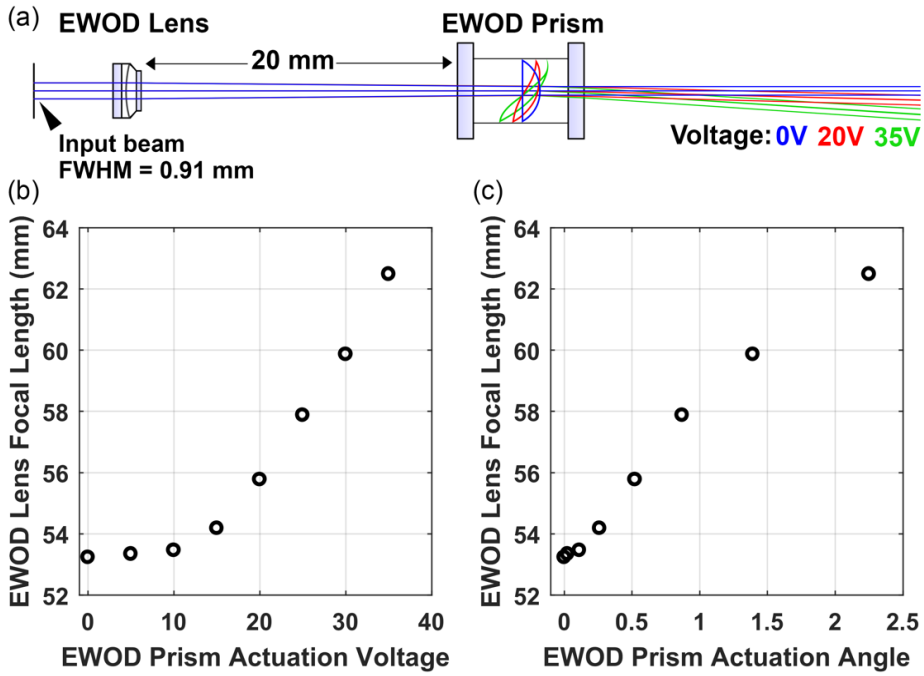

Fig. 5. (a) Zemax diagram of multi-configuration model of EWOD tunable focus lens (Varioptic Arctic 316) and EWOD prism showing three surface models of EWOD prism actuation at 0V, 20V, and 35V. Rays shown have a diameter of 0.91 mm FWHM. (b, c) Change in focal length setting on EWOD lens required to maintain the highest peak irradiance at the Gaussian focus after the objective lens, plotted as a function of EWOD actuation voltage (b) and EWOD scan actuation angle (c). EWOD = Electrowetting on dielectric, FWHM = Full width half max.

To evaluate the effect of the EWOD prism liquid-liquid interface and beam size on imaging quality, the system was modeled with Zemax optical design software. Figure 6(a) shows the cross-sections along the scanning axis of the focused Gaussian beam profiles as a function of lateral displacement. The normalized Y-axis maintains the relative peak irradiance of each Gaussian spot. The red-dashed lines show the focus from the larger beam (1.43 mm FWHM) without the Galilean telescope, and the black-dashed lines show the focus from the smaller beam (0.91 mm FWHM) reduced by the telescope. When compared to the smaller beam, the larger beam produces higher peak irradiance as a result of greater numerical aperture (NA) at the objective lens. However, the smaller beam performs better at higher scan angles. Figure 6(b) shows a more detailed two-dimensional profile of the Gaussian focus spots for the two beam sizes. The smaller beam (top) results in an overall large focus spot size at most scan angles, and becomes moderately distorted by astigmatic-like effects at higher EWOD voltages (>15V). In contrast, the larger beam is smaller and more tightly focused at lower actuation voltages, but at voltages > 25V it accumulates more aberrations, reducing its peak intensity. This is a result of aberrations introduced by the EWOD prism surface at higher scan angles, and this effect is more evident for the larger beam (1.43 mm FWHM) when compared to the smaller beam (0.91 mm FWHM). It is also important to understand the impact of the input beam size on the NA of the imaging system. Figure 6(c) shows the results of propagating beams of increasing diameter, up to 3.5 mm FWHM. Up to 2 mm, there is less than 1% loss of transmitted power (right axis, orange) due to clipping or other vignetting. However, the expected increase in imaging NA (left axis, blue) with beam size is halted at ~1.4 mm FWHM. This result suggests that the loss in imaging performance at high scan angles is not due to loss of transmitted power but is likely due to the accumulation of aberrations. These effects are more pronounced as the size of the input beam is increased.

Biomedical Optics EXPRESS

Based on these results, the imaging experiments were conducted with the Galilean telescope included in the system resulting in a beam with FWHM of 0.91 mm, resulting in a NA of 0.17 while maintaining a usable scan range of ~130µm through the system.

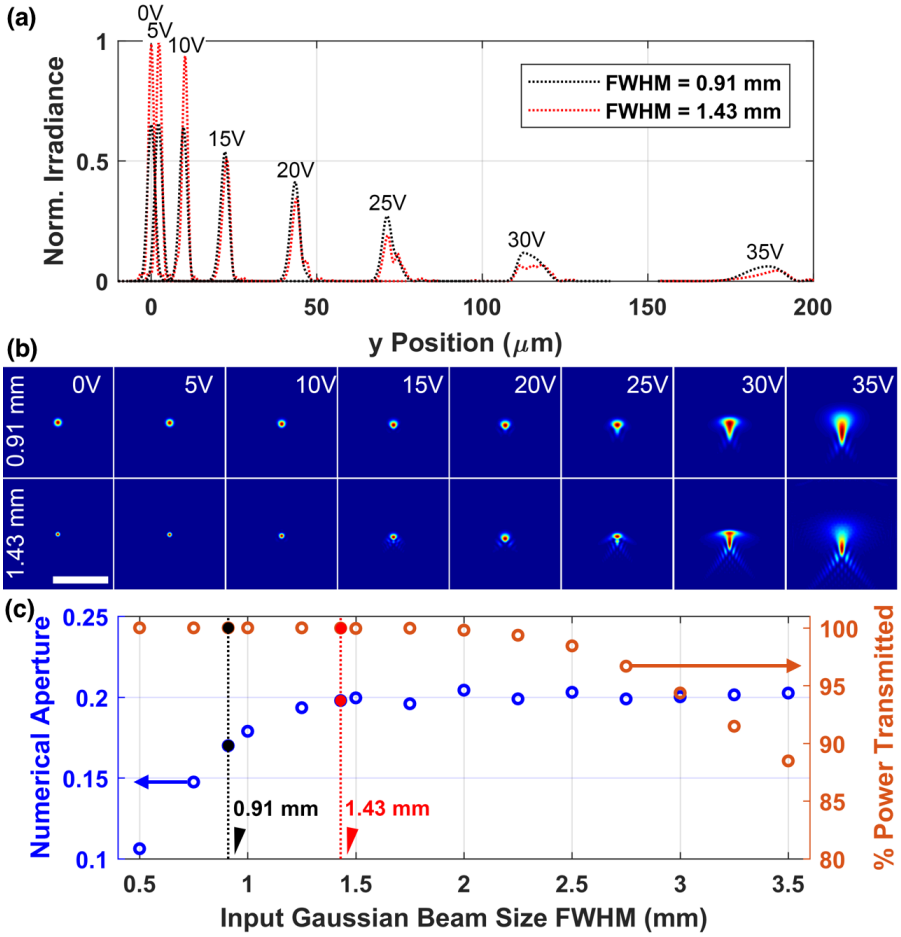

Fig. 6. (a) Lateral profiles of Gaussian beam foci, simulated in Zemax, as a function of increasing EWOD prism actuation voltage. The larger input beam (red-dashed, 1.43 mm FWHM) results in higher peak irradiance at low scan angles, while degrading faster than the smaller input beam (black-dashed, 0.91 mm FWHM) at higher EWOD prism voltages. (b) Transverse profiles of the simulated beam foci across voltage range. At larger scan angles, the beams are heavily aberrated in the EWOD prism scanning axis, resulting in reduced peak irradiance. Scale bar is 40 µm. (c) Focus-spot NA and power transmission through the Zemax model as a function of input beam size. EWOD prism is set to 0V. Beam sizes used in (a) and (b) are marked. The large beam size required to reduce power transmission suggests that optical aberrations, not clipping, is the main cause of the flattening of the NA increase curve. EWOD = Electrowetting on dielectric.

4.3 Device calibration using grid target

The voltage function shown in Eq. (2) was used to actuate the side-electrodes of the EWOD prism. While the function is determined using the steady state scan angle variation of the device, the scan angle variation still has some small time-dependent nonlinearity. This can be attributed to the time-dependent response of the EWOD prism upon actuation and an actuation delay introduced by the RC characteristics of the EWOD device [29]. Upon integration with the 2PE microscope, a scan range of ± 2° was obtained as a result of the physical implementation of the EWOD prism device.

Biomedical Optics EXPRESS

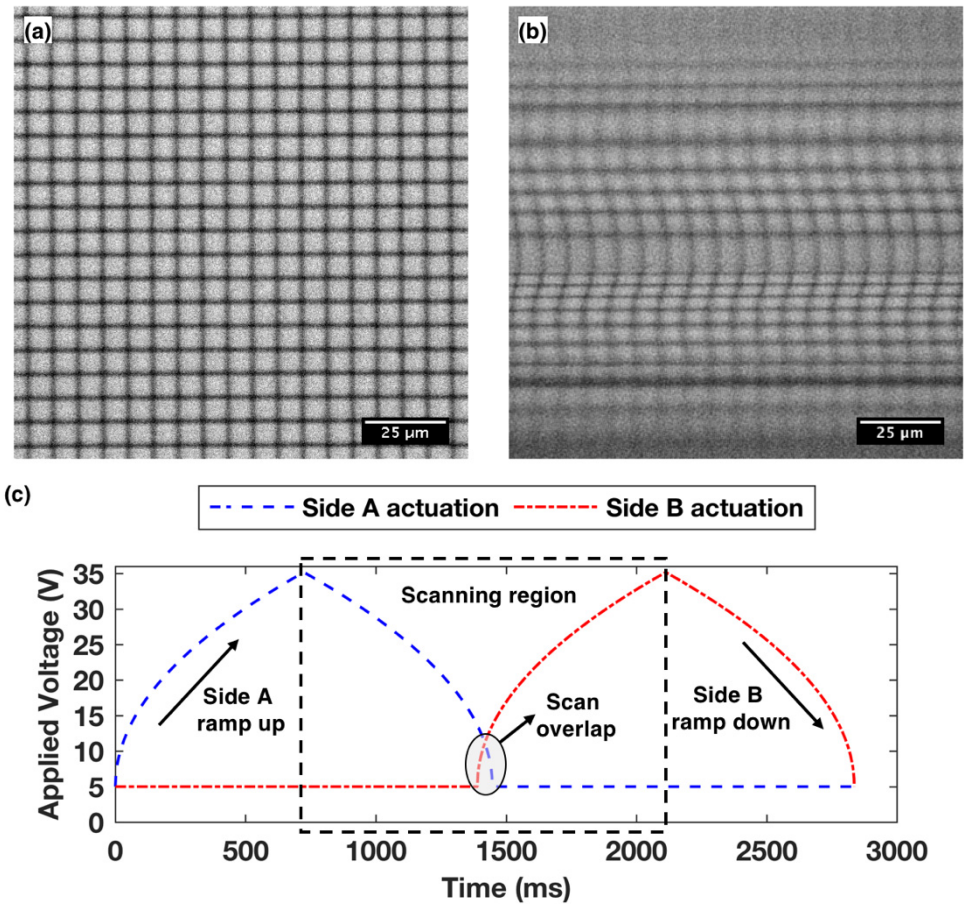

Fig. 7. (a) Image of the grid target acquired using galvo scanners, the grid spacing in the target is 7.5µm. (b) Image of the grid target acquired using EWOD prism raster scanning, the distortions are a result of non-linearity in the scan. (c) Actuation function used to drive the EWOD prism, the function shown in Eq. (2) is alternately applied to both electrodes.

In order to characterize this time-dependent scan angle nonlinearity of the device upon actuation with the voltage fit function (Eq. (2)), an image of a calibration grid target with a 7.5 µm grid spacing was obtained using the microscope. The calibration grid image was first taken, using conventional two-axis galvo scan mirrors with the EWOD prism in the path of the beam and actuation voltage set to V = 0 V. The EWOD lens, placed before the prism, was actuated at 44.5 V in order to compensate for the divergence of the EWOD prism and collimate the beam. This image (Fig. 7(a)) serves as a reference for calibrating the grid image with the EWOD prism. The reference calibration grid image was obtained at a resolution of 512 × 512 pixels with a dwell time of 10 µsec per pixel. An image of the calibration grid was then obtained by replacing one of the galvo mirror actuation axes with the EWOD prism (Fig. 7(b)), while keeping the pixel count and dwell time per pixel consistent with the reference calibration grid image. In this configuration, the EWOD prism serves as the slow axis scanner while the operational galvo mirror is used as the fast axis scanner for performing the raster scanning. The galvo mirror actuation range is set to ± 2V (corresponding to ± 2°) to match the scan range of the EWOD prism in the imaging system. The EWOD prism is actuated by applying the voltage function as described in Eq. (2) on the side-electrodes alternately with $\theta(t)$ linearly varying from between 0° to 2.35°. The scanning function starts with the first side-electrode at 35 V and the second side-electrode at 5V, and ends with the second side-

Biomedical Optics EXPRESS

electrode at 35 V and the first side-electrode at 5V. For this purpose, gradual ramp up and ramp down functions are included in the function to avoid oscillations at the liquid-liquid interface due to sudden actuation. The actuation voltage functions on the two side-electrodes are slightly overlapped at the transition in order to compensate for the time delay introduced by the RC characteristics of the device. A plot of the applied voltage function is shown in Fig. 7(c).

It is important to note that the curvature of the liquid-liquid interface changes upon actuation, causing the focal point of the objective to shift axially. To compensate for this effect, multiple scans were performed while reducing the EWOD lens actuation voltage 46.4V to 42.6V in steps of 0.2V per scan. The EWOD lens actuation voltage range from 42.6V to 46.4V covers the entire range of focal length shift (−63.2 mm to −52.8 mm) caused by the EWOD prism actuation. Using this technique only the regions in focus are resolved, leading to a stack of images with different parts of the target imaged depending on the focus of the system. Finally, the image of the target is constructed by taking z projection of the stack.

The warping in the image acquired by EWOD prism scanning can be corrected by applying a distortion correction matrix to the warped image. In order to generate the distortion correction matrix, the grid intersection points in both the reference grid image and the EWOD scanning image were first registered using the descriptor-based registration plugin in ImageJ software [30]. The coordinates of these intersection points were correlated between the images, and to map the intersection points from the EWOD prism scan to the reference image, a spline interpolant mapping function was determined. To correct for the image warping, the mapping function was then used to construct a transformation matrix in MATLAB, and applied to the grid image acquired using EWOD prism scan. Figure 8 shows the results from this image transformation. This transformation matrix serves as the basis for correcting for distortions in the 2PE images of fixed neuron cells.

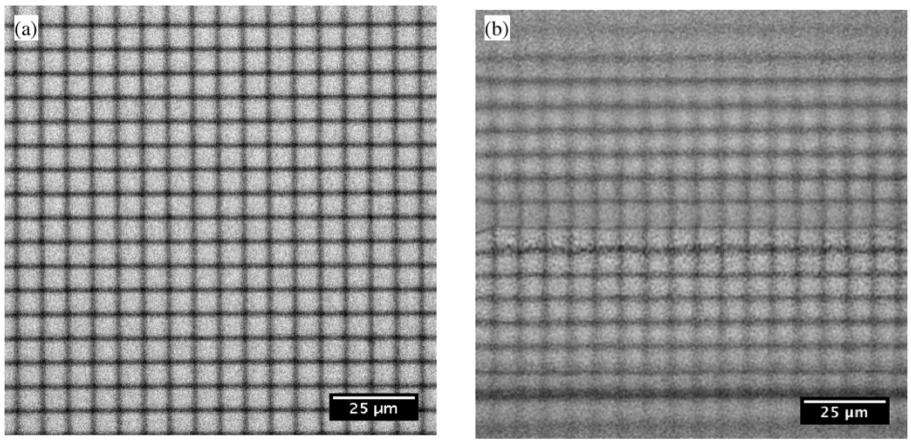

Fig. 8. (a) Image of the grid target acquired using galvo scanners, the grid spacing in the target is 7.5µm. (b) Image of the grid target acquired using EWOD prism raster scanning after distortion correction. The warping in the image is corrected by vector field mapping using a shape preserving spline interpolant function.

4.4 Two-photon imaging of hippocampus neuron cells

To demonstrate raster scanning for 2PE imaging of neurons, *in vitro* cultured mice hippocampus neurons labeled with enhanced green fluorescent proteins (eGFP) were used. The cultured cells were fixed with 4% paraformaldehyde and mounted on a glass slide to obtain a thin sample of cells for 2PE microscopy. The imaging was performed using single channel PMT detection corresponding to the emission from green fluorescent proteins. The

Biomedical Optics EXPRESS

same image acquisition protocol as the target grid pattern (described in section 4.3) was used to image the neurons. A reference image was acquired using galvo scanners prior to acquiring the cell image with the EWOD prism replacing one of the galvo mirrors as the slow axis scanner. Both the reference and EWOD prism scan images were acquired at an average laser input power of 9 mW at a resolution of 512 × 512 pixels with 10 µs dwell time per pixel. The focal length shift with the EWOD actuation is corrected passively by performing multiple scans with EWOD lens actuation voltage reduced from 46.4V to 42.6V in steps of 0.2V per scan, generating a stack of images containing different regions of the cell imaged while in focus. Due to enhanced sensitivity of 2PE at the focal point, individual images of the stacks produced are nearly free of background noise, and a maximum intensity projection of the image stack produces sharp image comparable to the quality of the image acquired using conventional galvo scanners. The images acquired using the EWOD prism are then corrected using the transformation matrix obtained from the grid target images. Figure 9 shows results of the cell images acquired using the EWOD prism scanning after distortion correction, and the reference image obtained using galvo scanners. It is evident from Fig. 9(c) that the image collected using EWOD prism scan upon distortion correction (Fig. 9(b)) resembles the reference image collected using the galvo scan (Fig. 9(a)) and that the cell shape is preserved on the EWOD prism scan image.

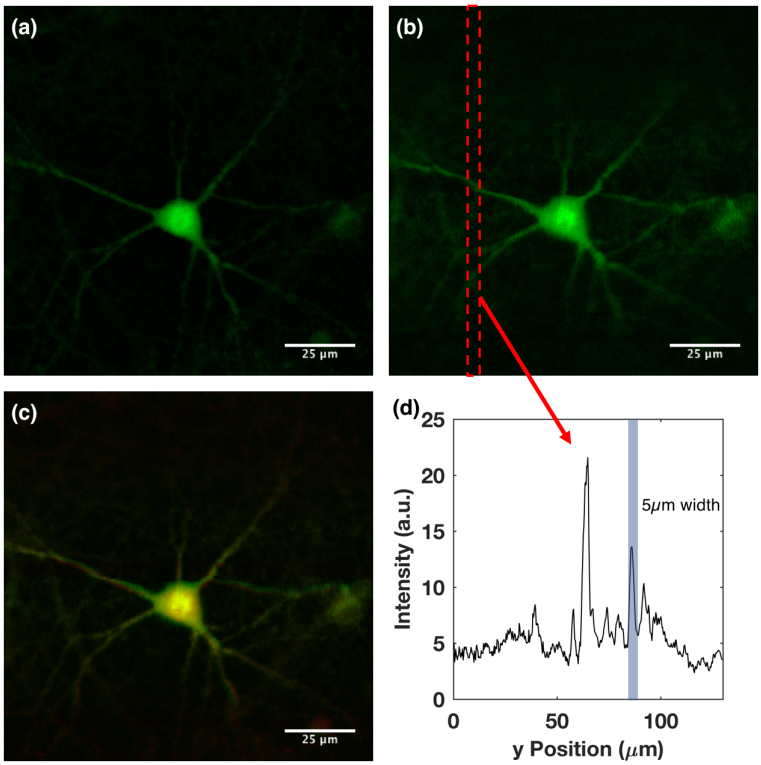

Fig. 9. (a) Image of a neuron collected using galvo scanners. (b) Image of the same neuron collected using EWOD prism scanning, the dotted box indicates the region of interest for image intensity plot (d). (c) Image (a) and (b) overlaid on top of each other, the red shade corresponds to the galvo scanned image, the green shade corresponds to the EWOD prism image, while yellow shade depicts the overlap region between the overlaid images. It can be clearly seen that the cell image preserving the cell shape can be recreated using the distortion correction matrix. (d) Image intensity cross section along y direction obtained from (b). Dendrites of the order of 5µm can be resolved in the image acquired using EWOD prism scanning.

Biomedical Optics EXPRESS

In addition to the cell body, the high-resolution images were even able to capture the fluorescence expression from dendrites with width of the order of 5μm. Images can be acquired faster using the EWOD prism scan by reducing the pixel count and dwell time for the scan. EWOD prism actuation of as fast as 21°/sec could be used to obtain lower resolution images. This actuation speed can be further improved by using techniques like voltage shaping [29] or resonance mode scanning, to reduce the scan time and implementation for fast axis scanning. The image shown in Fig. 9(b), acquired using the EWOD prism scanning indicates that the imaging system has a field of view (FOV) of 130 × 130 μm^2. This FOV is obtained using an input beam with a FWHM of 0.91 mm. The FOV of the imaging setup can be further enhanced by increasing the scan angle range of the EWOD prism by using a liquid system with a higher refractive index contrast. A higher resolution 2PE microscope image with a lower scan range can be acquired through this system by using a larger beam (1.43 mm FWHM). Also, the limitation imposed by aberrations through the EWOD prism on the scan range and the imaging quality can be decreased by either increasing the number of electrodes on the device resulting in a planar fluidic interface upon actuation [23], or with careful optical design incorporating wide angle steering optics [31] to enhance the scan range in the region where the effects of aberrations through the device are not pronounced.

5. Conclusion

We have demonstrated non-mechanical beam scanning in a 2PE microscope using a two electrode EWOD prism. This work of using transmissive adaptive optics using EWOD technology for high resolution 2PE microscopy paves the way for its implementation in miniature imaging optics for *in vivo* neuronal imaging of freely-behaving mice. This demonstration is a step towards a 2PE fiber-coupled system with integrated EWOD-based adaptive lateral and axial scanning.

We have demonstrated a process flow to fabricate two-electrode EWOD prism devices capable of providing repeatable and consistent scanning required for laser scanning microscopy. We have experimentally characterized the steady state scan angle range of the EWOD prism at ± 2.35° with an applied voltage of 35 V on the side-electrodes of the device. Using the scan angle variation of the device under applied voltage, we devised a driving voltage strategy for dynamic actuation of the device for integration in a conventional 2PE microscope.

The simulation results presented in this work describe in detail the critical parameters for the optical setup design for the EWOD prism integration. Using COMSOL Multiphysics, the liquid-liquid interface of the EWOD prism was simulated at various applied voltages. The surfaces obtained were imported in Zemax to simulate the Gaussian beam propagation through the EWOD prism and analyze the effect of the input beam size on critical imaging parameters such as NA, and scan range of the system. Based on the simulation results, a beam with FWHM of 0.91 mm was chosen to optimize the tradeoff between usable scan range and image resolution.

To the best of our knowledge, this work is the first to demonstrate the utility of EWOD prism devices as lateral scanning elements in 2PE microscopy. 2PE microscope images of fixed mouse hippocampus neurons were acquired through EWOD prism scanning, with the EWOD prism acting as the slow axis scanner. Images with preserved cell shape upon distortion correction and a FOV of 130 × 130 μm^2 were acquired using EWOD prism scanning. In addition to imaging the cell body, the images were also able to capture the fluorescence expression from the dendrites connected to the cell body.

Funding

This work was supported by the National Science Foundation (NSF) IDBR grant DBI-1353757, NSF NCS-FO grant CBET 1631704, National Institute of Health (NIH) SPARC grant OT2OD023852, and Office of Naval Research (ONR) grant N00014-15-1-2739.

Biomedical Optics EXPRESS

Publication of this article was funded by the University of Colorado Boulder Libraries Open Access Fund.

Acknowledgments

The authors acknowledge Prof. Ulli Bayer for providing cultured neuron samples. The authors are grateful to John Jackson from Metricon Corporation for refractive index measurements on the liquids. The authors also acknowledge Wei Yang Lim and Robert Cormack for fruitful discussions.

Disclosures

The authors declare that there are no conflicts of interest related to this article.